ACS Biomaterials SCIENCE & ENGINEERING
Article
Cite This: ACS Biomater. Sci. Eng. 2019, 5, 4463−4473
pubs.acs.org/journal/abseba

Nanomedicine Fabricated from A Boron-dipyrromethene (BODIPY)-Embedded Amphiphilic Copolymer for Photothermal-Enhanced Chemotherapy

Jie Shen,[*,†] Qiwen Wang,[‡] Yuanyuan Lv,[†] Jingyin Dong,[†] Guida Xuan,[†] Jie Yang,[*,§] Dan Wu,[⊥] Jiong Zhou,[§] Guocan Yu,[∥] Guping Tang,[⊥] Xiao Li,[*,▽,¶] Feihe Huang,[§] and Xiaoyuan Chen[*,∥]

[†]School of Medicine, Zhejiang University City College, Hangzhou 310015, P. R. China

[‡]Heart and Vascular Center, The First Affiliated Hospital, School of Medicine, Zhejiang University, Hangzhou, 310003 Zhejiang, P. R. China

[§]State Key Laboratory of Chemical Engineering, Center for Chemistry of High-Performance & Novel Materials, Department of Chemistry, Zhejiang University, Hangzhou 310027, P. R. China

[⊥]Department of Chemistry, Institute of Chemical Biology and Pharmaceutical Chemistry, Zhejiang University, Hangzhou 310027, P. R. China

[∥]Laboratory of Molecular Imaging and Nanomedicine, National Institute of Biomedical Imaging and Bioengineering, National Institutes of Health, Bethesda, Maryland 20892, United States

[▽]Women's Reproductive Health Laboratory of Zhejiang Province, Women's Hospital, Zhejiang University School of Medicine, Hangzhou, 310006 Zhejiang, China

[¶]The Department of Gynecologic Oncology, Women's Hospital, Zhejiang University School of Medicine, Hangzhou, 310006 Zhejiang, China

Supporting Information

ABSTRACT: To overcome the shortcomings of chemotherapy including side effects and uncontrollable release, as well as to increase the therapeutic efficacy, a diblock copolymer (mPEG-*b*-PLA-BODIPY) was constructed containing a NIR absorbing boron-dipyrromethene (BODIPY) tail, a hydrophobic polylactide (PLA) segment, and a hydrophilic poly(ethylene glycol) (PEG) segment. The nanoparticles self-assembled from mPEG-*b*-PLA-BODIPY with a core−shell structure were utilized to load docetaxel (DTX) in the core through hydrophobic interaction. Tailored drug release and high tumor penetration of the nanomedicine were realized by fully taking advantage of photothermal effect and the enhanced penetration and retention effect, facilitating enhanced therapeutic performance and reducing undesirable side effects. *In vivo* antitumor studies demonstrate that photothermal-enhanced chemotherapy effectively suppresses tumor progression, while systemic toxicity and side effects of DTX are remarkably decreased benefiting from rational design. This pioneering example provides a blueprint for the next generation of polymeric delivery vehicles integrating novel theranostic functions.

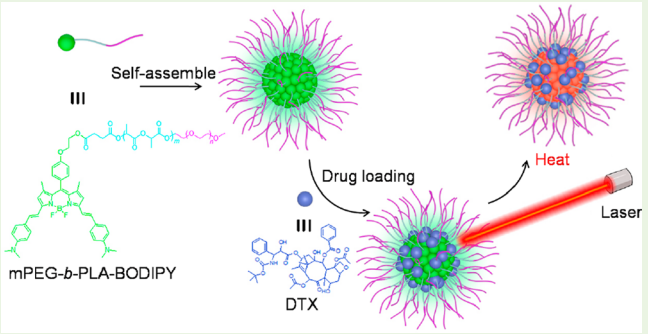

KEYWORDS: *photothermal effect, chemotherapy, BODIPY, docetaxel, lung cancer*

INTRODUCTION

Chemotherapy is considered to be one of the mainstays of clinical cancer treatment owing to its systemic efficacy and gratifying cytotoxicity. However, clinical applications of traditional chemotherapy are restricted by the serious side effects, such as myelosuppression, mucositis, alopecia, and peripheral neuropathy, because most of the low molecular weight chemotherapeutic drugs lack tumor targeting and thus also damage normal cells without specificity.[1−4] Over the past decades, nanomedicines have attracted tremendous attention from scientists to promote anticancer efficacy while overcoming the side effects of the drugs by specifically delivering the loaded drug to sites of action benefiting from the enhanced permeation and retention (EPR) effect. Among them, nanomedicines fabricated from copolymers especially exhibit distinct advantages including favorable biocompatibility and biodegradability,

Received: July 27, 2019
Accepted: August 12, 2019
Published: August 12, 2019

Downloaded via QUEEN MARY UNIV OF LONDON on March 3, 2022 at 15:33:40 (UTC).
See https://pubs.acs.org/sharingguidelines for options on how to legitimately share published articles.

ACS Publications © 2019 American Chemical Society

DOI: 10.1021/acsbiomaterials.9b01145
ACS Biomater. Sci. Eng. 2019, 5, 4463−4473

Scheme 1. Schematic Illustration of the Preparation of PPB/DTX Nanoparticles and the NIR Triggered Photothermal Adjunct Chemotherapy

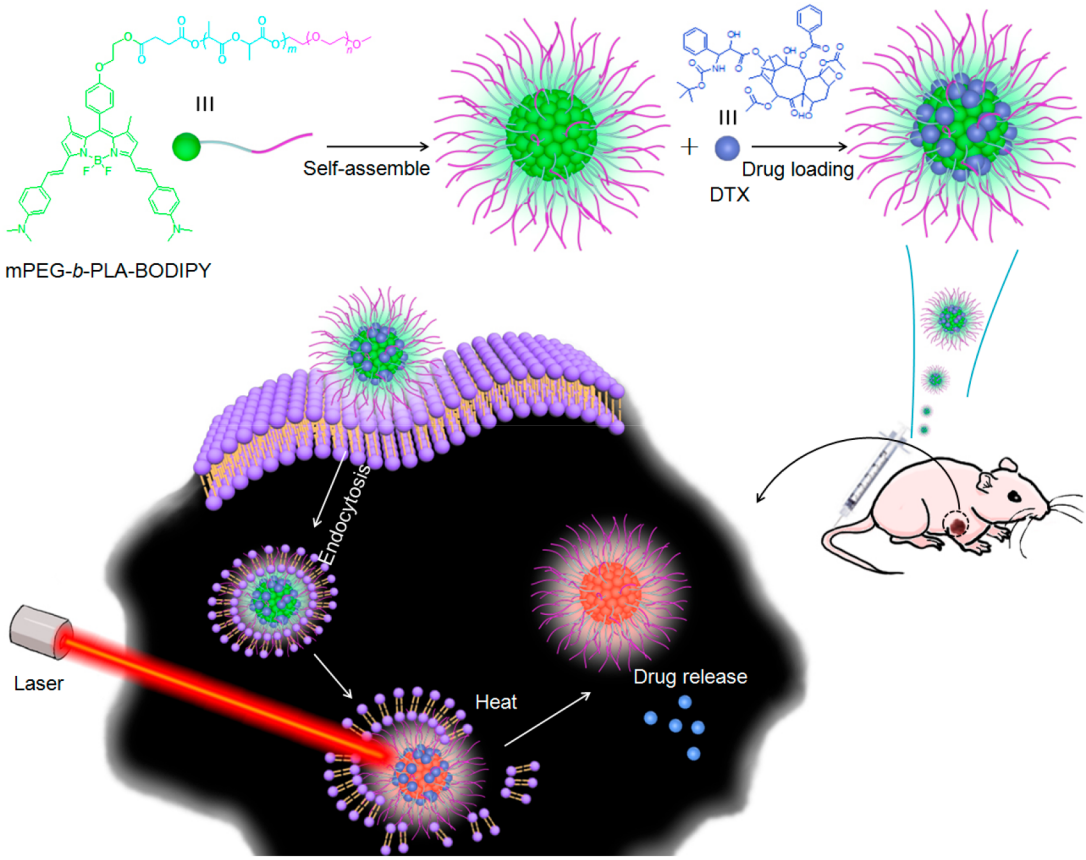

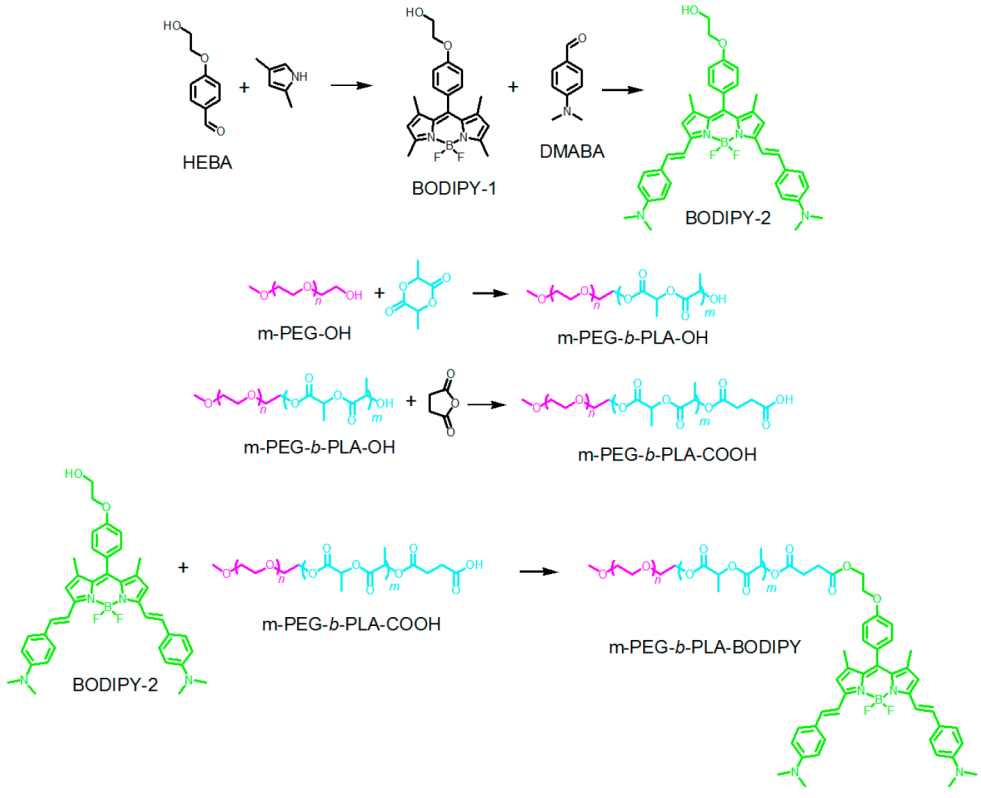

Figure 1. Synthetic route to mPEG-*b*-PLA-BODIPY.

DOI: 10.1021/acsbiomaterials.9b01145
ACS Biomater. Sci. Eng. 2019, 5, 4463−4473

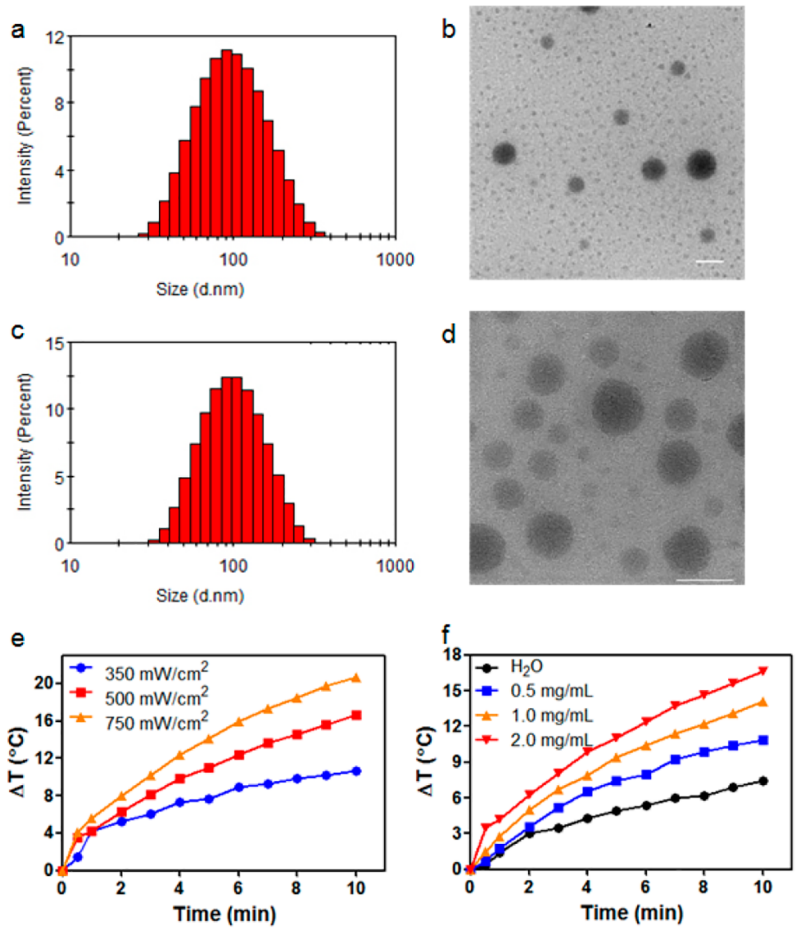

Figure 2. Characterization of PPB and PPB/DTX. DLS results and TEM images of (a, b) PPB nanoparticles and (c, d) PPB/DTX nanomedicine. Scale bar = 100 nm. (e) Photothermal curves of PPB at a concentration of 2.0 mg/mL. (f) Temperature changes of PPB in water irradiated with a NIR laser at a power density of 500 mW/cm^2 for 10 min.

improvement of drug solubility, minimization of side effects, prolongation of blood circulation time, and enhanced tumor accumulation.[5−13] Tailored drug release is another obstacle impeding the efficacy of chemotherapy, since the passive diffusion of most nanomedicines is inefficient and uncontrollable, always lowering the anticancer results and resulting in damage to normal organs. Therefore, the development of a sophisticated drug delivery system with spatial and temporal drug release ability is still highly desirable.[14,15]

Photothermal therapy (PTT), taking advantage of near-infrared (NIR) lasers and NIR absorbing agents to transduce NIR light into heat, has been developed as an attractive option for local tumor therapy.[16−21] Followed by flexible photothermal treatment, the release and tumor penetration of chemotherapeutic drugs can also be promoted because of the heat-induced disruption of the delivery system and the promotion of vascular permeability, making cancer cells more susceptible to chemotherapy.[22−26] Various photothermal agents have been developed for PTT and combination therapy, including gold nanorods or nanoparticles, carbon nanotubes, graphene oxide, indocyanine green, terrylenediimide, porphyrin, and aza-boron-dipyrromethene.[27−37] However, the majority of currently used inorganic PTT agents are not biodegradable and can remain inside the body for a long time, leading to potential long-term toxicity. In contrast, the organic PTT agents hold promising potential in clinical applications attributed to their excellent biocompatibility and biodegradability.[38−40]

In this work, a diblock copolymer (mPEG-*b*-PLA-BODIPY, PPB) containing a boron-dipyrromethene (BODIPY) tail, a hydrophobic polylactide (PLA) segment, and a hydrophilic poly(ethylene glycol) (PEG) segment was designed and successfully synthesized (Scheme 1). The BODIPY, which performs in a relatively narrow energy band gap, could exhibit strong absorbance in the NIR region and act as a photothermal agent. Driven by the hydrophobic interactions between drug and hydrophobic PLA segments, the chemotherapeutic drug docetaxel (DTX) can be encapsulated into the core of self-assembled nanoparticles from PPB. The obtained PPB/DTX nanoparticles demonstrate heat-controllable promotion of drug release in aqueous solution. The NIR-induced photothermal effect were able to increase the penetration of nanoparticles in a 3D multicellular spheroid of non-small-cell lung cancer A549 cells, exhibiting NIR-triggered intracellular drug accumulation. In addition, the antitumor efficacy of PPB/DTX was evaluated, indicating that the PPB drug delivery system was capable of enhancing the therapeutic efficacy of DTX. Following treatment with PPB/DTX and NIR irradiation, the growth of A549 xenografts obviously slowed down, revealing excellent antitumor effect of NIR triggered photothermal adjunct chemotherapy.

DOI: 10.1021/acsbiomaterials.9b01145
ACS Biomater. Sci. Eng. 2019, 5, 4463−4473

RESULTS AND DISCUSSION

Synthesis and Characterization of PPB Copolymer. The synthetic route to PPB is shown in Figure 1. First, BODIPY-1 was obtained from a two-step reaction starting from 1,4-hydroxyethoxybenzaldehyde (HEBA) and 2,4-dimethyl pyrrole, which further reacted with dimethylaminobenzaldehyde to afford BODIPY-2. For the preparation of mPEG-*b*-PLA-COOH, a ring-opening polymerization of lactide was adopted using mPEG-OH as a macromolecular initiator followed by the reaction with succinic anhydride with a yield of ∼85% in two steps. The amphiphilic diblock copolymer PPB was obtained through esterification between mPEG-*b*-PLA-COOH and BODIPY-2. Various characterizations were applied to confirm the successful synthesis of the PPB (Figures S1−S8). ^{1}H NMR and ^{13}C NMR spectra provided direct evidence for the preparation of BODIPY-2. According to the ^{1}H NMR spectrum of mPEG-*b*-PLA-OH (Figure S6), the molecular weight was calculated to be 14.4 kDa. In the gel permeation chromatography (GPC) curves (Figure S5), the mPEG-*b*-PLA-OH copolymer showed a monomodal pattern with a polydispersity of 1.11, suggesting a well-controlled polymerization of the product. Moreover, the structure of PPB was also confirmed by ^{1}H NMR spectrum (Figure S8), showing proton peaks of BODIPY ranging from 6.7 to 7.7 ppm. The amphiphilic PPB with a hydrophobic core composed of PLA and BODIPY, and a hydrophilic PEG segment was able to self-assemble into stable nanoparticles. The particle size of PPB was characterized by dynamic light scattering (DLS). The average hydrodynamic diameter of the PPB nanoparticles was 86.3 ± 0.7 nm (Figure 2a). Transmission electron microscopy (TEM) of PPB showed a spherical structure, which dispersed uniformly with a diameter of approximately 100 nm (Figure 2b). The UV−vis spectrum of PPB indicated an intense absorption between 600 and 800 nm (Figure S9), confirming the photothermal capability of this delivery vehicle.

To confirm the photothermal effect, we monitored the temperature change of the solution containing PPB at a concentration of 2.0 mg/mL upon laser irradiation at 670 nm with different power density. Figure 2e showed that the photothermal efficiency of PPB was laser power intensity dependent. However, irradiation with the 670 nm laser at a density of 750 mW/cm^2 for 10 min had obvious influence on cell viability (Figure S11). The cell viability decreased to 58.0% ± 8.8% when the power density increased from 500 to 750 mW/cm^2. Therefore, the optimal power density was kept at 500 mW/cm^2 for further study.

As observed in Figure 2f, exposure of the PPB polymer to the 670 nm laser at a power density of 500 mW/cm^2 for 10 min produced a concentration-dependent increase of the temperature by 10.9, 14.1, and 16.6 °C for PPB concentration of 0.5, 1.0, and 2.0 mg/mL, respectively. Thus, the excellent photothermal efficiency of PPB demonstrated above showed great potential in photothermal-enhanced chemotherapy.

Preparation and Characterization of DTX Loaded PPB Nanoparticles. With this potential photothermal polymer in hand, we introduced docetaxel (DTX) as the chemotherapeutic drug. The microtubule-stabilizing drug DTX is applied to many types of cancers in clinical practice, including breast cancer, lung cancer, and ovarian cancer. However, the clinical use of DTX is greatly limited by its poor aqueous solubility (6−7 μg/mL).[41−44] To improve the solubility of DTX, DTX loaded PPB nanoparticles (PPB/DTX) were successfully prepared by hydrophobic interaction using the solvent evaporation method. The average size of PPB/DTX in aqueous solution characterized by DLS, as shown in Figure 2c, is 85.4 ± 0.6 nm in diameter. The TEM images provided visual morphological evidence showing the stable formation of PPB/DTX sphere with a diameter of approximately 100 nm (Figure 2d). The results of DLS and TEM demonstrated negligible influence on the formation and size of nanoparticles upon loading DTX in comparison with PPB nanoparticles. Since mPEG-*b*-PLA (PP) micellar nanodrugs are widely studied and some are commercially available, such as Genexol-PM, the advantage of BODIPY conjugated mPEG-*b*-PLA in drug loading was evaluated. As shown in Table 1, in comparison with PP, the BODIPY conjugated copolymer PPB exhibited remarkably higher drug loading contents (LC), indicating that the conjugated BODIPY, which was utilized as a photothermal agent, also contributed to formation of nanomedicine through enhanced hydrophobic interaction.

Table 1. Drug Loading Capability Evaluations

	polymer (mg)	DTX (mg)	EE[a] (%)	LC[b] (%)
PP	10.0	2.0	74.5	13.0
	10.0	3.0	70.8	17.5
	10.0	4.0	64.7	20.5
	10.0	5.0	65.8	24.8
	10.0	6.0	64.2	27.8
PPB	10.0	2.0	90.9	15.4
	10.0	3.0	89.9	21.2
	10.0	4.0	92.1	26.9
	10.0	5.0	93.7	31.9
	10.0	6.0	86.7	34.2

[a]Encapsulation efficiency (EE) = $m_{load}/m_{add} \times 100\%$, where m_{add} and m_{load} represent the drug mass added during the preparation of drug-loaded nanoparticles (NPs) and that loaded by the NPs, respectively. [b]Loading content (LC) = $m_{load}/(m_{load} + m) \times 100\%$, where m represents the mass of polymer used during the preparation of drug-loaded NPs.

The stability of copolymers in biological buffers was studied by DLS. The results implied that both nanoparticles self-assembled from PP and those from PPB were stable in PBS and DMEM containing 10% serum (Figure 3a,b), confirming the long-circulating characteristic of obtained nanoparticles in biological conditions.

The *in vitro* drug release of PPB/DTX were tested under different conditions. During the drug release experiments, tween 80 (0.5% w/v) was added into the dissolution medium for the poorly soluble DTX to maintain a sink state. As shown in Figure 3c and Figure S10, only a small portion of drug was released from the PPB/DTX NPs in the presence of serum, and the release rate of PPB/DTX was slower than that of PP/DTX at 37 °C, indicating better stability of PPB/DTX and a lower risk of drug leakage for PPB/DTX nanomedicine in further *in vivo* applications compared with PP/DTX. Additionally, drug release at 44 °C which was reported to be effective for thermosensitization,[45,46] was faster than that at 37 °C, indicating that the photothermal effect promotes drug release, which can facilitate release of the loaded drug at the site of activity, thus reducing side effects of the nanomedicines.

The hemolysis assay was carried out to assess whether the PPB copolymer would destroy red blood cells (RBCs). Figure 3d shows the hemolysis rates of PPB in various concentrations ranging from 50 to 2000 μg/mL at different incubation times.

DOI: 10.1021/acsbiomaterials.9b01145
ACS Biomater. Sci. Eng. 2019, 5, 4463−4473

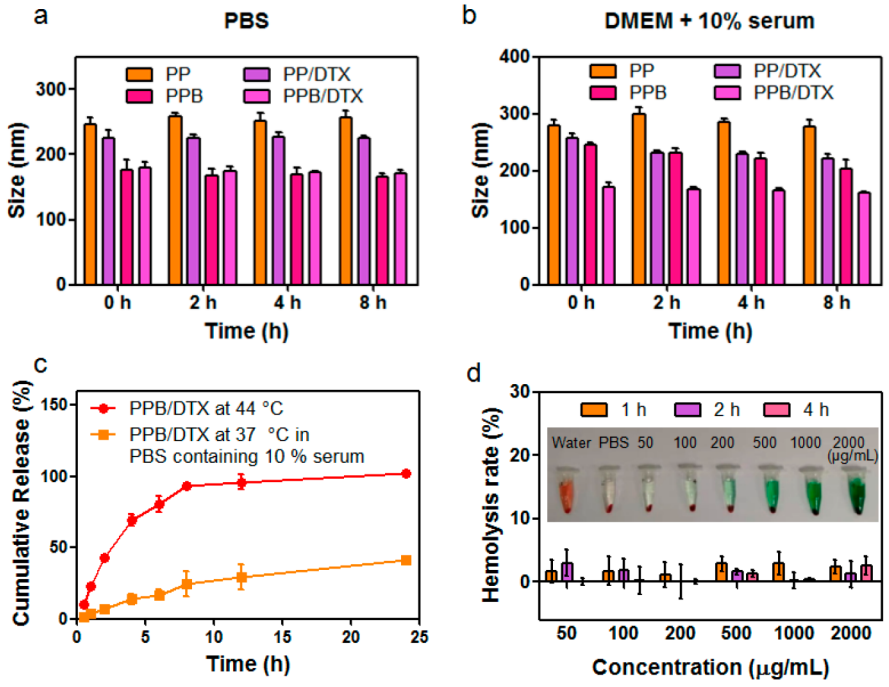

Figure 3. Stability of PP, PP/DTX, PPB, and PPB/DTX in (a) PBS and (b) DMEM containing 10% serum. (c) Drug release of PPB/DTX at the temperature of 44 and 37 °C. (d) Hemolysis assay of PPB. Various concentrations of PPB from 50 to 2000 μg/mL were incubated with red blood cells for 1, 2, and 4 h. The deionized water was used as a positive control, and PBS was used as a negative control (n = 3).

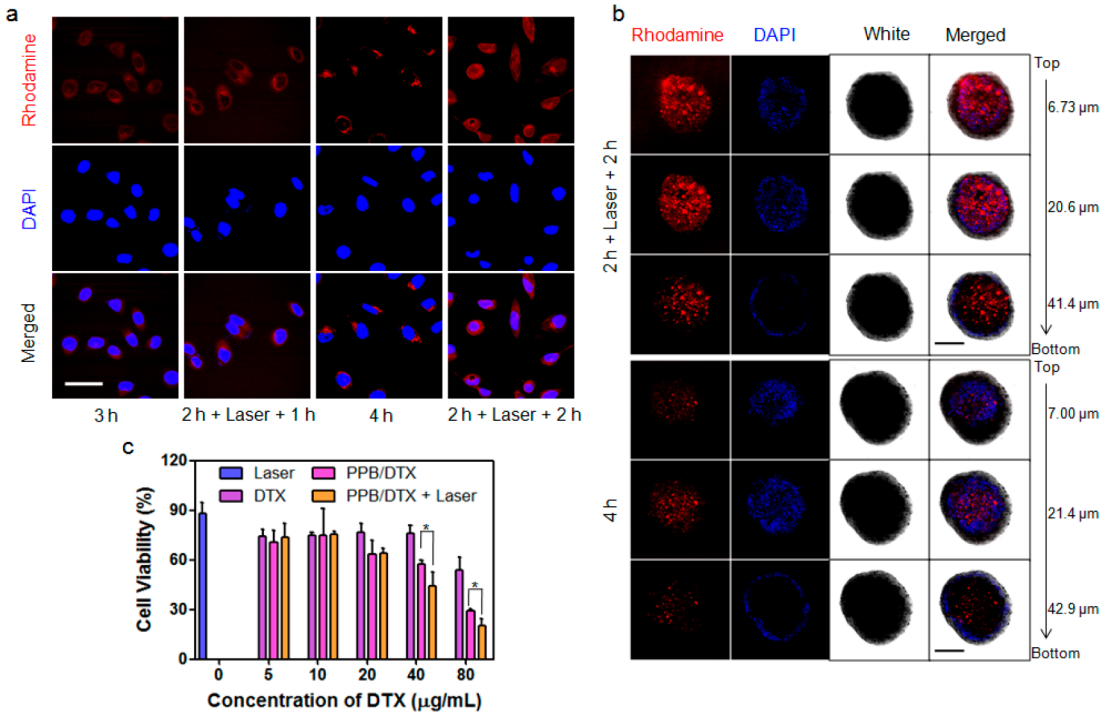

Figure 4. (a) Fluorescence images of A549 cells treated with PPB/Rho (2.0 mg/mL) for a total of 3 or 4 h, where the PPB/Rho is shown in red, and the nucleus is stained with DAPI. Scale bar = 50 μm. (b) Penetration of PPB/Rho nanoparticles into 3D-cultured A549 tumor spheroids for 4 h imaged with a confocal laser scanning microscope. The representative confocal images were taken at 7, 21, and 42 μm from the spheroid rim. Scale bar = 200 μm. (c) Cell viability of A549 cells treated with laser, free DTX, PPB/DTX, and PPB/DTX + laser at different concentrations of DTX. Data represent mean ± SD (n = 3) (Student's t test, *p < 0.05).

PPB copolymer only induced a hemolysis rate of 2.6% ± 1.4% after 4 h incubation when the concentration of PPB was as high as 2000 μg/mL, implying its good hemocompatibility. Therefore, PPB/DTX, integrating features of high loading contents, excellent stability and hemocompatibility, and heat-induced controlled drug release, showed great potential for further studies.

DOI: 10.1021/acsbiomaterials.9b01145
ACS Biomater. Sci. Eng. 2019, 5, 4463−4473

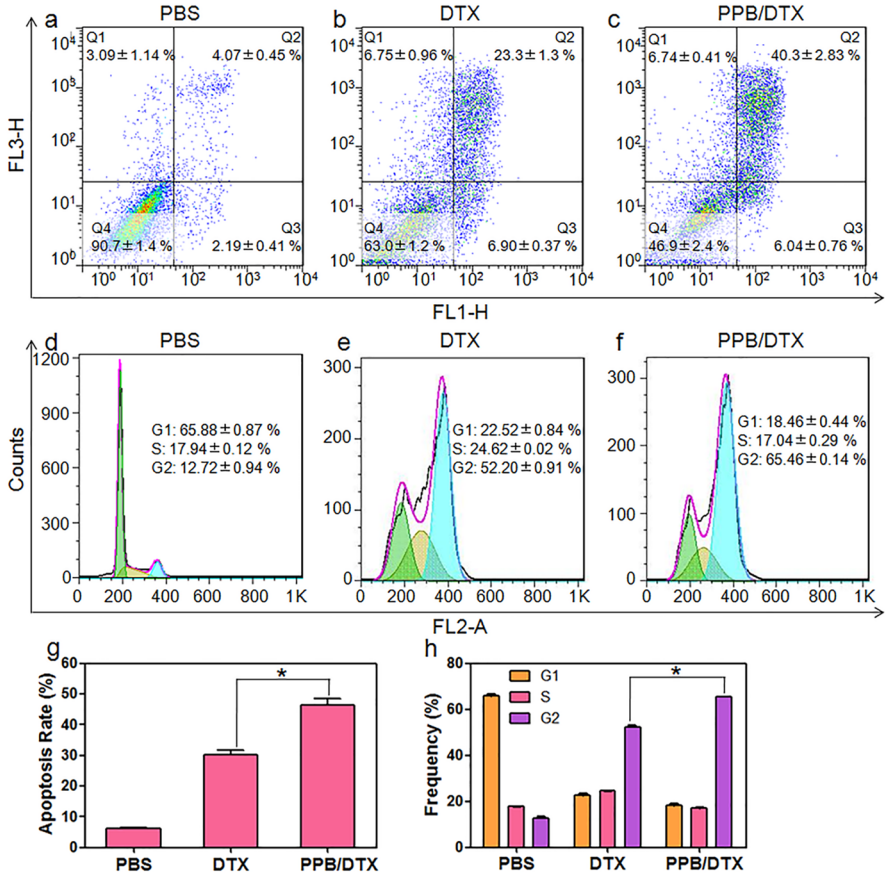

Figure 5. Apoptosis analysis (a, b, c) and cell cycle (d, e, f) of A549 cells treated with different formulations at a DTX concentration of 0.1 μg/mL. The quantitative analysis was calculated by flow cytometry. Data represent mean ± SD (n = 3). (g) Total apoptosis rate (Q2 + Q3) of A549 cells after treatment with PBS, DTX, or PPB/DTX for 48 h incubation (Student's t test, *p < 0.05). (h) Frequency of G0/G1 phase, S phase, and G2/M phase of A549 cells after treatment with PBS, DTX, or PPB/DTX for 48 h incubation (Student's t test, *p < 0.05).

Cellular Uptake and Antitumor Activities of DTX Loaded PPB Nanoparticles. The PPB nanoparticles showed good encapsulation ability and excellent drug release behavior; however, good *in vitro* biocompatibility is also necessary for the PPB polymer to be further applied in tumor therapy. Therefore, *in vitro* cytotoxicity was evaluated using the 3-(4′,5′-dimethylthiazol-2′-yl)-2,5-diphenyltetrazolium bromide (MTT) assay on human non-small-cell lung cancer A549 cells. As shown in Figure S12, satisfactory biocompatibility of PPB was revealed by MTT assay, demonstrating high cell viability after treatment with different concentrations of PPB. Subsequently, *in vitro* cellular uptake and anticancer efficacy were tested on A549 cells. It has been reported that photothermal treatment contributes to cellular uptake.[47] In order to obtain visible results, the cellular uptake assay was performed with rhodamine B as a red fluorescent probe. The images in Figure 4a show the cellular uptake of rhodamine B loaded PPB (PPB/Rho) on A549 cells after 3 or 4 h and show that the application of laser irradiation caused an increase of red fluorescence, which suggested promotion of cellular uptake. The penetration of nanoparticles into the solid tumor tissues is one of the main challenges for the effective tumor therapy. To further assess the penetration ability, we carried out a cellular uptake experiment in a three-dimensional (3D) model with A549 cells, which mimics the microenvironment and morphology of solid tumors.[48,49] The images were scanned layer by layer using confocal laser scanning microscopy to monitor the penetration of PPB/Rho nanoparticles into the 3D multicellular spheroid (MCS). As shown in Figure 4b, the red fluorescence of PPB/Rho was observed deeper and more intensely in the MCS with the assistance of laser irradiation, indicating that the hyperthermia triggered by irradiation of PPB significantly enhanced the penetration and accumulation of nanoparticles into deep tumors.

Besides the heat-induced penetration, we were also interested in exploring whether the bioavailability and antitumor activity of DTX could be improved with the PPB/DTX nanomedicine formulation. To this end, the anticancer efficacy of DTX was evaluated by MTT assay. Figure 4c shows the cell viability of A549 cells under treatment with free DTX, PPB/DTX, and PPB/DTX combined 10 min laser irradiation. The efficacy of DTX was significantly improved when the PPB/DTX was irradiated with the NIR laser, suggesting photothermally enhanced chemotherapy. Moreover, the PPB/DTX nanomedicine formulation demonstrated higher efficacy than free DTX. The result was further confirmed by a cell apoptosis assay and cell circle experiment. In the cell apoptosis assay, the cells were treated with various formulations at a DTX concentration of 0.1 μg/mL for 48 h, and cell apoptosis was quantified using an Annexin V-FITC/PI apoptosis detection kit (Figure 5a–c). Q2 and Q3 in the plots represent late apoptotic cells and early apoptotic cells, respectively, whereas Q4 represents normal cells, and Q1 represents necrotic cells. The treatment with PPB/DTX obviously induced higher rates of cell apoptosis (Q2 + Q3, 46.4% ± 2.1%) than treatment with free DTX (30.2% ± 1.6%) (p < 0.05), implying that the cell apoptosis was enhanced after

DOI: 10.1021/acsbiomaterials.9b01145
ACS Biomater. Sci. Eng. 2019, 5, 4463–4473

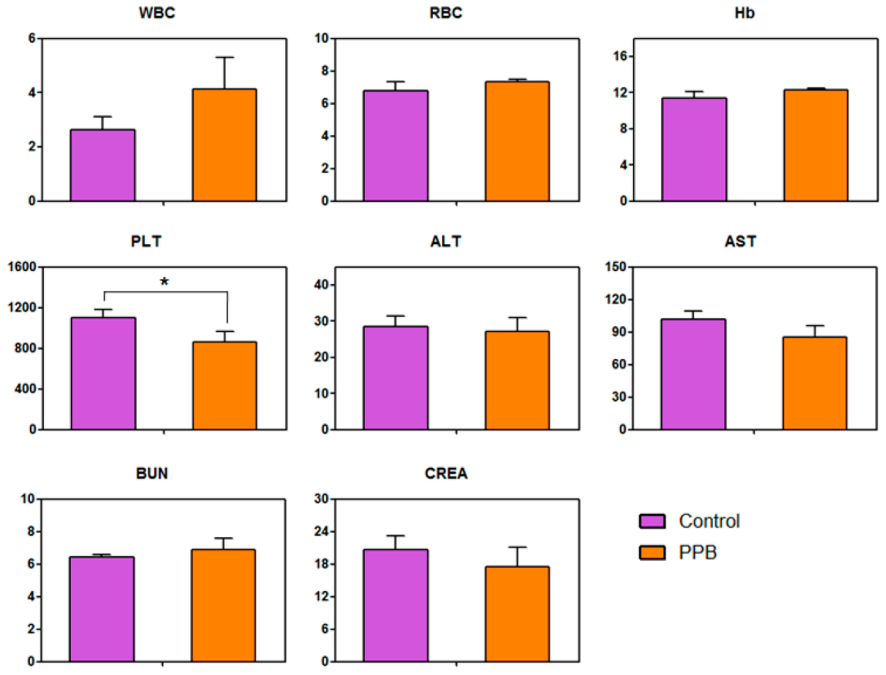

Figure 6. Blood test parameters for mice treated with PBS or PPB through iv injection. Data are shown as mean ± SD ($n = 3$) (Student's t test, $^*p < 0.05$). Blood routine examination includes white blood cell (WBC), red blood cell (RBC), hemoglobin (Hb), and blood platelet (PLT), liver function includes alanine aminotransferase (ALT) and aspartate aminotransferase (AST), and kidney function includes blood urea nitrogen (BUN) and creatinine (CREA).

the encapsulation of DTX by PPB. This result was also supported by the cell cycle experiments (Figure 5d–f). The DTX inhibited microtubule disassembly and arrested cells in G2/M phase. As expected, we found higher G2/M phase arrest with PPB/DTX. Compared to that with free DTX, the frequency of cells in G2/M phase with PPB/DTX treatment was increased from 52.20% ± 0.91% to 65.46% ± 0.14% ($p < 0.05$), indicating better antiproliferative activity.

***In Vivo* Therapeutic Efficacy of DTX Loaded PPB Nanoparticles.** Given the excellent anticancer activity, PPB was further employed for *in vivo* studies. First, the *in vivo* safety of PPB copolymer was evaluated using ICR mice. Routine blood examination, liver function, and kidney function of mice were evaluated after intravenous injection with PPB once every 2 days for four times. Compared to the control group with PBS injection, the blood test parameters of mice treated with PPB exhibited no significant differences, except a little decrease of PLT (Figure 6), revealing the good biocompatibility of PPB. To explore the biodistribution of PPB/DTX in mice, DTX extracted from different organs including lung, liver, spleen, kidney, heart, and tumor after intravenous injection with PPB/DTX for 6, 12, 24, or 48 h was quantified using HPLC. Free DTX was used as control. As shown in Figure 7a,b, after 6 h postinjection, free DTX was found to accumulate mostly in lung as a result of the interception of insoluble DTX. The amount of DTX in tumor tissue decreased as time progressed. At 48 h postinjection, DTX was hardly detected in all organs, which demonstrated that free DTX could be quickly cleared from the body. However, the biodistribution of DTX changed upon the injection of PPB/DTX nanomedicine. At 12 h postinjection, DTX was found at the highest concentrations in most tissues including lung, liver, spleen, and tumor, verifying that the biodistribution of PPB/DTX nanomedicine was different from free DTX. Benefiting from the EPR effect and the long-circulation capability of PPB/DTX nanomedicine, the amount of DTX in tumor remained relatively high even 48 h postinjection, thereby enhancing antitumor effect of DTX.

The *in vivo* photothermal properties were investigated using tumor-bearing BALB/c nude mice. PBS and PPB polymer were injected into the tumor-bearing mice, and then mice were treated with a 670 nm laser at 500 mW/cm^2 for 10 min. The thermography is provided in Figure S13; in comparison with PBS, the administration of PPB polymer followed by laser irradiation successfully increased temperature to 44 °C at the tumor site, confirming the good photothermal efficiency of PPB *in vivo*. Figure S14 shows the *in vivo* tumor penetration of PPB/Rho with and without laser irradiation. Frozen sections were taken every 200 μm from the top to the bottom. The red fluorescence in the tumor only treated with PPB/Rho could be observed until the sixth section, whereas that in the tumor treated with both PPB/Rho and laser was stronger until the eighth section, suggesting enhanced *in vivo* penetration with the photothermal effect.

Afterward, the *in vivo* tumor suppression experiment was carried out to confirm the cancer treatment potential of PPB/DTX nanomedicine. Mice bearing A549 xenografts were treated with PPB/DTX and various other formulations by intravenous injection once every 2 days for 7 days at an equivalent DTX dose of 5 mg/kg. Tween-80 was also used to help solubilize free DTX.[50,51] As shown in Figure 7c,d, the administration of PBS with and without laser irradiation, which was used as negative control, allowed rapid tumor growth, suggesting negligible tumor suppression. Similarly, the hyperthermia induced by laser exposure in PPB treated mice hardly limited the tumor growth. As DTX has been already proved to be effective in lung cancer, free DTX treatment demonstrated efficacy in tumor inhibition as did PPB/DTX treatment. However, PPB/DTX treatment exhibited significantly better tumor suppression due to the

DOI: 10.1021/acsbiomaterials.9b01145
ACS Biomater. Sci. Eng. 2019, 5, 4463–4473

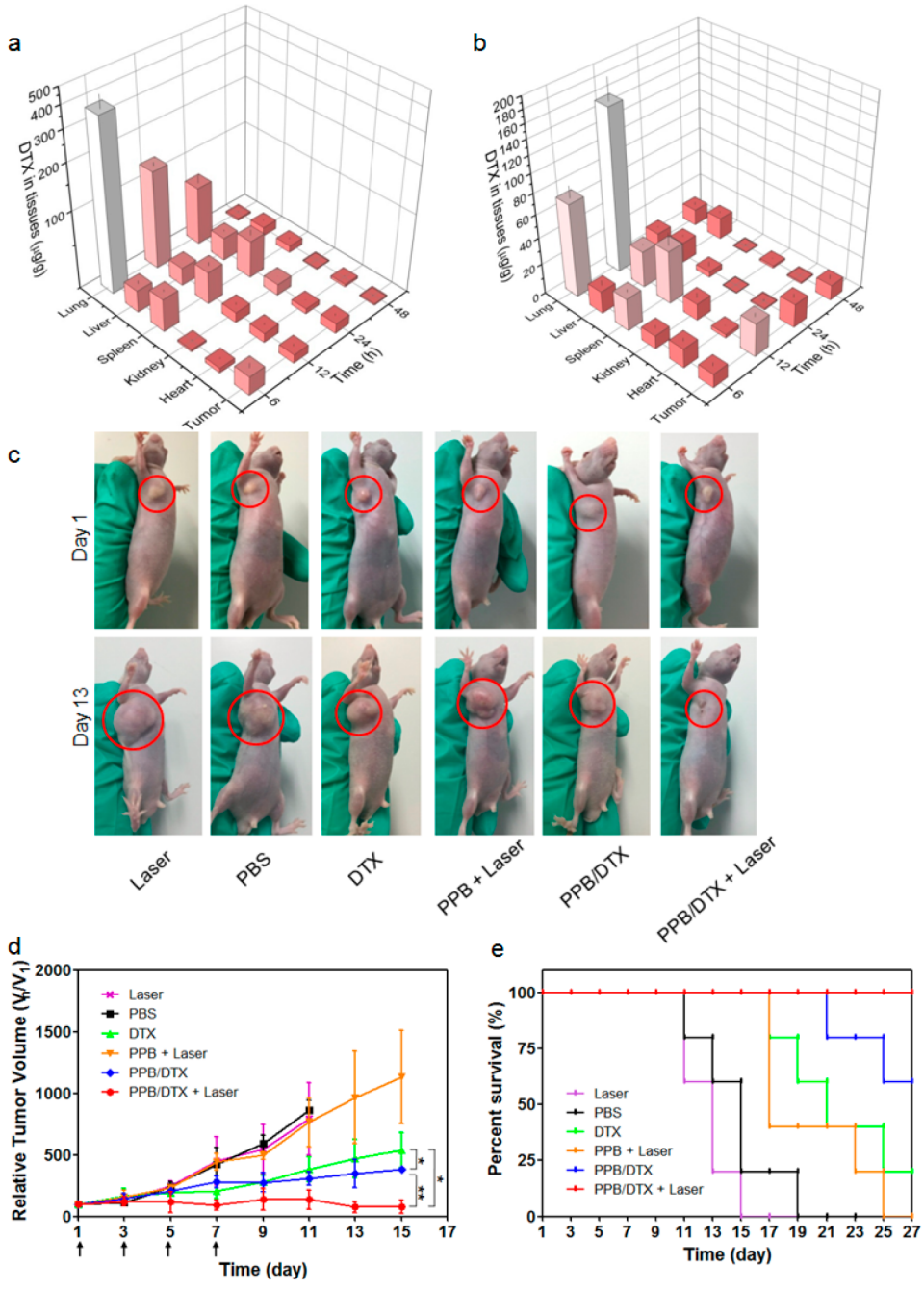

Figure 7. Quantitative analysis of DTX acquired from tumors and various organs at 6, 12, 24, and 48 h after intravenous injection of (a) free DTX and (b) PPB/DTX ($n = 3$). (c) Images of in vivo tumor growth. (d) Relative tumor volume curves of BALB/c nude mice bearing A549 xenografts after the treatments of the indicated formulations. Data represent mean ± SD ($n = 5$) (Student's t test, $^{**}p < 0.01$, $^{*}p < 0.05$). (e) Survival curves of BALB/c nude mice bearing A549 xenografts after the different treatments ($n = 5$).

higher tumor accumulation and long-circulating time of the PPB/DTX nanomedicine. Notably, the relative tumor volume was inhibited most efficiently by treatment with PPB/DTX followed by laser irradiation. This observation indicated that the PPB drug delivery system could effectively deliver DTX to the tumor, and the synergy of chemotherapy and photothermia could significantly inhibit the tumor growth in a more efficient manner. The survival curves of mice were recorded (Figure 7e). The PPB/DTX + laser group had a 100% survival rate during the experimental period, verifying the high efficiency of photothermal PPB/DTX system. Furthermore, as shown in Figure S15, the H&E stained tumor tissue appeared hypercellular and showed nuclear polymorphism. The results of Ki-67 staining assay utilized to assess tumor proliferation showed a lower Ki-67 level in the PPB/DTX + laser group than those in other groups, illustrating that cell proliferation in tumors treated with PPB/DTX and laser irradiation was lower. The results of TUNEL assay proved that the PPB/DTX nanoparticles with laser irradiation lead to more cell apoptosis than other formulations. These observations implied that the high antitumor activity was induced by cell apoptosis and inhibition of cell proliferation by PPB/DTX nanomedicine with laser irradiation. The body

DOI: 10.1021/acsbiomaterials.9b01145
ACS Biomater. Sci. Eng. 2019, 5, 4463−4473

weights of mice were recorded and analyzed. As shown in Figure S16, the recovery of body weight in the PPB/DTX + laser group was observed to be faster than that of the DTX group, implying lower systemic toxicity and side effects of DTX encapsulated by the PPB drug delivery system. Moreover, the histopathology of organs including heart, liver, and kidney of PPB/DTX + laser group were studied. Compared with the PBS-treated mice, no obvious inflammatory lesions or tissue damage was observed in the major organs, further confirming the low systemic toxicity of PPB/DTX + laser combination (Figure S17).

CONCLUSION

We developed a BODIPY-based amphiphilic polymer, which could be applied as an insoluble drug delivery system and produce a NIR laser-induced hyperthermia. Benefiting from the hydrophobic interaction, the PPB copolymer and DTX could form stable nanoparticles in aqueous solution and biological buffers with a satisfactory drug loading content. The photothermal capability of the nanomedicine promoted drug release, facilitating improved anticancer efficacy and reducing undesirable side effects. The cellular uptake studies demonstrated the relation between laser-induced hyperthermia and penetration in both 2D and 3D cell models. Irradiation with the NIR laser obviously contributed to penetration and accumulation of drugs in solid tumors. The cytotoxicity, cell apoptosis, and cell cycle studies demonstrated the efficient anticancer ability of the PPB/DTX nanomedicine. *In vivo* study showed the good biocompatibility and successful photothermal effect of PPB in tumor-bearing mice. The biodistribution of DTX verified the long-circulating time and EPR effects of PPB/DTX. The tumor suppression study provided direct evidence for the potential application of the photothermal PPB/DTX system for cancer treatment. The current study confirms a novel photothermal drug delivery system, which can effectively combine photothermia and chemotherapy, providing the possibility for polymeric delivery vehicles integrating novel theranostic functions.

EXPERIMENTAL SECTION

Evaluation of Photothermal Properties. The PPB aqueous solution at concentrations of 0.5, 1.0, and 2.0 mg/mL was irradiated with a 670 nm laser at 500 mW/cm^2. Temperatures were measured for a total of 10 min with a thermal imaging camera (Fotric 326, Fotric, USA). In addition, the PPB aqueous solution at a concentration of 2.0 mg/mL was irradiated with a 670 nm laser at 350, 500, and 750 mW/cm^2, and the temperature was measured as described above.

Evaluation of Hemolysis. Red blood cells (RBCs) were collected from ICR mice. The blood sample, treated with anticoagulant, was diluted with PBS and centrifuged at 1500 rpm for 10 min at 4 °C. The erythrocytes at the bottom of the centrifuged sample were isolated and washed three times with 1× PBS. The diluted RBCs were incubated with different concentrations of PPB solution for 1, 2, and 4 h at 37 °C. Deionized water and PBS were used as the positive and negative controls, respectively. The corresponding samples were centrifuged at 5000 rpm for 10 min. To assess the hemolysis rate, the absorbance of the supernatant at 540 nm was measured. The hemolysis rate was calculated using the following formula: hemolysis rate (%) = $[(A_{sample} - A_0)/(A_{100} - A_0)] \times 100\%$, where A_{sample}, A_{100}, and A_0 represent the absorbance of the sample, deionized water, and PBS, respectively.

Cellular Uptake Study. The cellular uptake of PPB with or without laser treatment was studied using confocal laser scanning microscopy (CLSM, FV1000, Olympus, Tokyo, Japan) with rhodamine B as a fluorescent probe. PPB/Rho was prepared by the solvent evaporation method. A549 cells were seeded in 24-well plates with cell slides and grown for 18 h. The medium was changed to serum-free DMEM containing PPB/Rho (at a concentration of 2 mg/mL). After 2 h incubation, the laser treatment groups were irradiated with a 670 nm laser at 500 mW/cm^2 for 10 min. The cells were then incubated for another 1 or 2 h at 37 °C. The control group was incubated without laser for 3 or 4 h. The cell slides were rinsed with PBS, fixed with fresh 4% paraformaldehyde, and stained with DAPI for 10 min.

3D *in Vitro* Model Study. A549 cells were seeded on 96-well plates and centrifuged at 300 × g for 10 min. Then the cells were incubated for 3 days to grow into a 500 μm diameter 3D cell culture model. The 3D models were incubated with serum-free DMEM containing PPB/Rho (at a concentration of 2.0 mg/mL) for 2 h, then irradiated with the laser for 10 min, and incubated for another 2 h. The control groups were incubated without laser irradiation. The 3D models were rinsed with PBS, stained with DAPI for 30 min, and scanned with confocal laser scanning microscopy (CLSM, FV1000, Olympus, Tokyo, Japan).

Animal Experiments. For the blood test, ICR mice were treated with PPB via intravenous injection (60 mg/kg) once every 2 days for 4 times. PBS was used as control. After treatment, the mice were sacrificed, and the blood samples were collected and sent to the Center for Drug safety Evaluation and Research of ZJU.

To study the biodistribution of DTX, tumor bearing BALB/c nude mice were treated with free DTX and PPB/DTX through the tail vein and then sacrificed 6, 12, 24, and 48 h after injection. The organs were suspended in acetonitrile, homogenated, and filtered. DTX concentration was subsequently quantified by HPLC. The mobile phase consisted of acetonitrile and water (55:45). The chromatographic conditions were as follows: an ultraviolet detector set at 230 nm; a C18 column (4.6 mm × 150 mm, ZORBAX SB-C18, Agilent, Santa Clara, CA, USA) operated at 25 °C ± 1.0 °C, and a flow rate of 0.6 mL/min.

To evaluate the photothermal effect of PPB, BALB/c nude mice bearing A549 xenogenic tumors were anesthetized 1 h after subcutaneous injection of PPB (2.0 mg/mL in PBS) or an equal volume of PBS. Then the tumors of mice were irradiated with a 670 nm laser at 500 mW/cm^2 for 10 min, and the temperatures were subsequently recorded using a photothermal imaging camera (Fotric 326, Fotric, USA).

For the *in vivo* tumor penetration experiment, after the tumor bearing BALB/c mice were subcutaneously injected with PPB/Rho and the appropriate groups were subsequently treated with laser irradiation, the mice were sacrificed, and the tumors were embedded in O.C.T. compound (SAKURA Tissue-Tek) at −85 °C. Frozen sections were taken every 200 μm from the top to the bottom, each section being 20 μm thick. The images were taken using a fluorescence microscope (Nikon Ts2R, Nikon, Japan).

For the tumor suppression study, the tumor bearing BALB/c mice were assigned to six groups and treated with PBS, laser, PPB, DTX, PPB/DTX, PPB with laser, and PPB/DTX with laser (laser irradiations were performed 12 h after injection) at 5 mg/kg equivalent DTX via intravenous injection once every 2 days for 4 times. The tumor volume was measured by a caliper once every 2 days and calculated by the following formula: tumor volume V (mm^3) = 1/2 × length (mm) × width^2 (mm^2); relative tumor volume = V_n/V_1. The body weight of mice was recorded. After treatment, the mice were sacrificed, and the tumors and organs were fixed with 4% paraformaldehyde, dehydrated, and embedded in paraffin. The slices were stained with hematoxylin and eosin (H&E) according to a standard protocol. The expression levels of Ki-67 were evaluated using immunohistochemical staining. The apoptosis of tumor cells was investigated by the TUNEL method. The photos were scanned and read by the CaseViewer software (3DHISTECH, Budapest, Hungary).

ASSOCIATED CONTENT

Supporting Information

The Supporting Information is available free of charge on the ACS Publications website at DOI: 10.1021/acsbiomaterials.9b01145.

Experimental details, characterization of materials, in vitro drug release data, cytotoxicity evaluation, in vivo

DOI: 10.1021/acsbiomaterials.9b01145
ACS Biomater. Sci. Eng. 2019, 5, 4463−4473

photothermal effect, in vivo tumor penetration, histopathology and immunohistochemistry of tumors, body weight analysis of treated mice, and histopathology of mouse organs (PDF)

AUTHOR INFORMATION

Corresponding Authors

*E-mail: shenj@zucc.edu.cn.
*E-mail: jieyang@zju.edu.cn.
*E-mail: 5198008@zju.edu.cn.
*E-mail: shawn.chen@nih.gov.

ORCID

Yuanyuan Lv: 0000-0003-4736-3733
Jie Yang: 0000-0001-9970-7505
Guping Tang: 0000-0003-3256-740X
Feihe Huang: 0000-0003-3177-6744

Notes

The authors declare no competing financial interest.

ACKNOWLEDGMENTS

This work was supported by the National Natural Science Foundation of China (51603184 and 81800442), Zhejiang Postdoctor Research Project (zj20180129), and China Postdoctoral Science Foundation funded project (2019M652121).

REFERENCES

(1) Krukiewicz, K.; Zak, J. K. Biomaterial-based regional chemotherapy: Local anticancer drug delivery to enhance chemotherapy and minimize its side-effects. *Mater. Sci. Eng., C* **2016**, *62*, 927−942.

(2) Teoh, D.; Smith, T. J.; Song, M.; Spirtos, N. M. Care After Chemotherapy: Peripheral Neuropathy, Cannabis for Symptom Control, and Mindfulness. *Am. Soc. Clin Oncol Educ Book* **2018**, No. 38, 469−479.

(3) Hauner, K.; Maisch, P.; Retz, M. [Side effects of chemotherapy]. *Urologe A* **2017**, *56* (4), 472−479.

(4) Beaver, C. C.; Magnan, M. A. Managing Chemotherapy Side Effects: Achieving Reliable and Equitable Outcomes. *Clin J. Oncol Nurs* **2016**, *20* (6), 589−591.

(5) Wu, X.; Zhou, L.; Su, Y.; Dong, C. M. Plasmonic, Targeted, and Dual Drugs-Loaded Polypeptide Composite Nanoparticles for Synergistic Cocktail Chemotherapy with Photothermal Therapy. *Biomacromolecules* **2016**, *17* (7), 2489−2501.

(6) Wu, D.; Li, Y.; Shen, J.; Tong, Z.; Hu, Q.; Li, L.; Yu, G. Supramolecular chemotherapeutic drug constructed from pillararene-based supramolecular amphiphile. *Chem. Commun. (Cambridge, U. K.)* **2018**, *54* (59), 8198−8201.

(7) Li, Y.; Bai, H.; Wang, H.; Shen, Y.; Tang, G.; Ping, Y. Reactive oxygen species (ROS)-responsive nanomedicine for RNAi-based cancer therapy. *Nanoscale* **2018**, *10* (1), 203−214.

(8) Wu, M.; Liu, X.; Jin, W.; Li, Y.; Hu, Q.; Chu, P. K.; Tang, G.; Ping, Y.; Li, Y. Targeting ETS1 with RNAi-based supramolecular nanoassemblies for multidrug-resistant breast cancer therapy. *J. Controlled Release* **2017**, *253*, 110−121.

(9) Guo, Z.; Zou, Y.; He, H.; Rao, J.; Ji, S.; Cui, X.; Ke, H.; Deng, Y.; Yang, H.; Chen, C.; Zhao, Y.; Chen, H. Bifunctional Platinated Nanoparticles for Photoinduced Tumor Ablation. *Adv. Mater.* **2016**, *28* (46), 10155−10164.

(10) Leung, M. H.; Harada, T.; Dai, S.; Kee, T. W. Nanoprecipitation and Spectroscopic Characterization of Curcumin-Encapsulated Polyester Nanoparticles. *Langmuir* **2015**, *31* (42), 11419−11427.

(11) Qiu, M.; Zhang, Z. Q.; Wei, Y. H.; Sun, H. L.; Meng, F. H.; Deng, C.; Zhong, Z. Y. Small-Sized and Robust Chimaeric Lipopepsomes: A Simple and Functional Platform with High Protein Loading for Targeted Intracellular Delivery of Protein Toxin in Vivo. *Chem. Mater.* **2018**, *30* (19), 6831−6838.

(12) Shanmugam, V.; Chien, Y. H.; Cheng, Y. S.; Liu, T. Y.; Huang, C. C.; Su, C. H.; Chen, Y. S.; Kumar, U.; Hsu, H. F.; Yeh, C. S. Oligonucleotides-Assembled Au Nanorod-Assisted Cancer Photothermal Ablation and Combination Chemotherapy with Targeted Dual-Drug Delivery of Doxorubicin and Cisplatin Prodrug. *ACS Appl. Mater. Interfaces* **2014**, *6* (6), 4382−4393.

(13) Zhu, A. J.; Miao, K.; Deng, Y. B.; Ke, H. T.; He, H.; Yang, T.; Guo, M.; Li, Y. L.; Guo, Z. Q.; Wang, Y. Y.; Yang, X. L.; Zhao, Y. L.; Chen, H. B. Dually pH/Reduction-Responsive Vesicles for Ultrahigh-Contrast Fluorescence Imaging and Thermo-Chemotherapy-Synergized Tumor Ablation. *ACS Nano* **2015**, *9* (8), 7874−7885.

(14) Gao, H.; Bi, Y.; Chen, J.; Peng, L. R.; Wen, K. K.; Ji, P.; Ren, W. F.; Li, X. Q.; Zhang, N.; Gao, J. M.; Chai, Z. F.; Hu, Y. Near-Infrared Light-Triggered Switchable Nanoparticles for Targeted Chemo/Photothermal Cancer Therapy. *ACS Appl. Mater. Interfaces* **2016**, *8* (24), 15103−15112.

(15) Yuan, A.; Huan, W.; Liu, X.; Zhang, Z. C.; Zhang, Y. F.; Wu, J. H.; Hu, Y. Q. NIR Light-Activated Drug Release for Synergetic Chemo-Photothermal Therapy. *Mol. Pharmaceutics* **2017**, *14* (1), 242−251.

(16) Liu, Y. W.; Bai, J.; Jia, X. D.; Jiang, X. E.; Guo, Z. Fabrication of Multifunctional SiO2@GN-Serum Composites for Chemo-Photothermal Synergistic Therapy. *ACS Appl. Mater. Interfaces* **2015**, *7* (1), 112−121.

(17) Ren, F.; Bhana, S.; Norman, D. D.; Johnson, J.; Xu, L. J.; Baker, D. L.; Parrill, A. L.; Huang, X. H. Gold Nanorods Carrying Paclitaxel for Photothermal-Chemotherapy of Cancer. *Bioconjugate Chem.* **2013**, *24* (3), 376−386.

(18) Zeng, X. W.; Luo, M. M.; Liu, G.; Wang, X. S.; Tao, W.; Lin, Y. X.; Ji, X. Y.; Nie, L.; Mei, L. Polydopamine-Modified Black Phosphorous Nanocapsule with Enhanced Stability and Photothermal Performance for Tumor Multimodal Treatments. *Adv. Sci.* **2018**, *5* (10), 1800510.

(19) Cheng, W.; Nie, J. P.; Gao, N. S.; Liu, G.; Tao, W.; Xiao, X. J.; Jiang, L. J.; Liu, Z. G.; Zeng, X. W.; Mei, L. A Multifunctional Nanoplatform against Multidrug Resistant Cancer: Merging the Best of Targeted Chemo/Gene/Photothermal Therapy. *Adv. Funct. Mater.* **2017**, *27* (45), 1704135.

(20) Peng, Y. M.; Nie, J. P.; Cheng, W.; Liu, G.; Zhu, D. W.; Zhang, L. H.; Liang, C. Y.; Mei, L.; Huang, L. Q.; Zeng, X. W. A multifunctional nanoplatform for cancer chemo-photothermal synergistic therapy and overcoming multidrug resistance. *Biomater. Sci.* **2018**, *6* (5), 1084−1098.

(21) Liu, S. C.; Pan, J. M.; Liu, J. X.; Ma, Y.; Qiu, F. X.; Mei, L.; Zeng, X. W.; Pan, G. Q. Dynamically PEGylated and Borate-Coordination-Polymer-Coated Polydopamine Nanoparticles for Synergetic Tumor-Targeted, Chemo-Photothermal Combination Therapy. *Small* **2018**, *14* (13), 1703968.

(22) Yu, G.; Yang, Z.; Fu, X.; Yung, B. C.; Yang, J.; Mao, Z.; Shao, L.; Hua, B.; Liu, Y.; Zhang, F.; Fan, Q.; Wang, S.; Jacobson, O.; Jin, A.; Gao, C.; Tang, X.; Huang, F.; Chen, X. Polyrotaxane-based supramolecular theranostics. *Nat. Commun.* **2018**, *9* (1), 766.

(23) Wust, P.; Hildebrandt, B.; Sreenivasa, G.; Rau, B.; Gellermann, J.; Riess, H.; Felix, R.; Schlag, P. M. Hyperthermia in combined treatment of cancer. *Lancet Oncol.* **2002**, *3* (8), 487−497.

(24) Urano, M.; Kuroda, M.; Nishimura, Y. For the clinical application of thermochemotherapy given at mild temperatures. *Int. J. Hyperthermia* **1999**, *15* (2), 79−107.

(25) Beik, J.; Abed, Z.; Ghoreishi, F. S.; Hosseini-Nami, S.; Mehrzadi, S.; Shakeri-Zadeh, A.; Kamrava, S. K. Nanotechnology in hyperthermia cancer therapy: From fundamental principles to advanced applications. *J. Controlled Release* **2016**, *235*, 205−221.

(26) Huilgol, N. G.; Gupta, S.; Sridhar, C. R. Hyperthermia with radiation in the treatment of locally advanced head and neck cancer: a report of randomized trial. *J. Cancer Res. Ther* **2010**, *6* (4), 492−496.

(27) Guo, B.; Sheng, Z.; Hu, D.; Li, A.; Xu, S.; Manghnani, P. N.; Liu, C.; Guo, L.; Zheng, H.; Liu, B. Molecular Engineering of Conjugated Polymers for Biocompatible Organic Nanoparticles with Highly Efficient Photoacoustic and Photothermal Performance in Cancer Theranostics. *ACS Nano* **2017**, *11* (10), 10124−10134.

DOI: 10.1021/acsbiomaterials.9b01145
ACS Biomater. Sci. Eng. 2019, 5, 4463−4473

(28) Liu, Y.; Yang, M.; Zhang, J.; Zhi, X.; Li, C.; Zhang, C.; Pan, F.; Wang, K.; Yang, Y.; Martinez de la Fuentea, J.; Cui, D. Human Induced Pluripotent Stem Cells for Tumor Targeted Delivery of Gold Nanorods and Enhanced Photothermal Therapy. *ACS Nano* **2016**, *10* (2), 2375−2385.
(29) Yang, Q.; Peng, J.; Xiao, Y.; Li, W.; Tan, L.; Xu, X.; Qian, Z. Porous Au@Pt Nanoparticles: Therapeutic Platform for Tumor Chemo-Photothermal Co-Therapy and Alleviating Doxorubicin-Induced Oxidative Damage. *ACS Appl. Mater. Interfaces* **2018**, *10* (1), 150−164.
(30) Huang, P.; Bao, L.; Zhang, C.; Lin, J.; Luo, T.; Yang, D.; He, M.; Li, Z.; Gao, G.; Gao, B.; Fu, S.; Cui, D. Folic acid-conjugated silica-modified gold nanorods for X-ray/CT imaging-guided dual-mode radiation and photo-thermal therapy. *Biomaterials* **2011**, *32* (36), 9796−9809.
(31) Thapa, R. K.; Youn, Y. S.; Jeong, J. H.; Choi, H. G.; Yong, C. S.; Kim, J. O. Graphene oxide-wrapped PEGylated liquid crystalline nanoparticles for effective chemo-photothermal therapy of metastatic prostate cancer cells. *Colloids Surf., B* **2016**, *143*, 271−277.
(32) Zhang, S.; Guo, W.; Wei, J.; Li, C.; Liang, X. J.; Yin, M. Terrylenediimide-Based Intrinsic Theranostic Nanomedicines with High Photothermal Conversion Efficiency for Photoacoustic Imaging-Guided Cancer Therapy. *ACS Nano* **2017**, *11* (4), 3797−3805.
(33) Yu, J.; Javier, D.; Yaseen, M. A.; Nitin, N.; Richards-Kortum, R.; Anvari, B.; Wong, M. S. Self-assembly synthesis, tumor cell targeting, and photothermal capabilities of antibody-coated indocyanine green nanocapsules. *J. Am. Chem. Soc.* **2010**, *132* (6), 1929−1938.
(34) Lv, G.; Guo, W.; Zhang, W.; Zhang, T.; Li, S.; Chen, S.; Eltahan, A. S.; Wang, D.; Wang, Y.; Zhang, J.; Wang, P. C.; Chang, J.; Liang, X. J. Near-Infrared Emission CuInS/ZnS Quantum Dots: All-in-One Theranostic Nanomedicines with Intrinsic Fluorescence/Photoacoustic Imaging for Tumor Phototherapy. *ACS Nano* **2016**, *10*, 9637−9645.
(35) Liu, Y.; Song, N.; Chen, L.; Liu, S.; Xie, Z. Synthesis of a Near-Infrared BODIPY Dye for Bioimaging and Photothermal Therapy. *Chem. - Asian J.* **2018**, *13* (8), 989−995.
(36) Yao, X. X.; Tian, Z. F.; Liu, J. X.; Zhu, Y. F.; Hanagata, N. Mesoporous Silica Nanoparticles Capped with Graphene Quantum Dots for Potential Chemo-Photothermal Synergistic Cancer Therapy. *Langmuir* **2017**, *33* (2), 591−599.
(37) Cao, M. J.; Wang, P. Y.; Kou, Y.; Wang, J.; Liu, J.; Li, Y. H.; Li, J. Y.; Wang, L. M.; Chen, C. Y. Gadolinium(III)-Chelated Silica Nanospheres Integrating Chemotherapy and Photothermal Therapy for Cancer Treatment and Magnetic Resonance Imaging. *ACS Appl. Mater. Interfaces* **2015**, *7* (45), 25014−25023.
(38) Zhang, Y. Y.; Ang, C. Y.; Li, M. H.; Tan, S. Y.; Qu, Q. Y.; Zhao, Y. L. Polymeric Prodrug Grafted Hollow Mesoporous Silica Nanoparticles Encapsulating Near-Infrared Absorbing Dye for Potent Combined Photothermal-Chemotherapy. *ACS Appl. Mater. Interfaces* **2016**, *8* (11), 6869−6879.
(39) Li, D. D.; Wang, J. X.; Ma, Y.; Qian, H. S.; Wang, D.; Wang, L.; Zhang, G. B.; Qiu, L. Z.; Wang, Y. C.; Yang, X. Z. A Donor-Acceptor Conjugated Polymer with Alternating Isoindigo Derivative and Bithiophene Units for Near-Infrared Modulated Cancer Thermo-Chemotherapy. *ACS Appl. Mater. Interfaces* **2016**, *8* (30), 19312−19320.
(40) Zhu, Y. D.; Chen, S. P.; Zhao, H.; Yang, Y.; Chen, X. Q.; Sun, J.; Fan, H. S.; Zhang, X. D. PPy@MIL-100 Nanoparticles as a pH- and Near-IR-Irradiation-Responsive Drug Carrier for Simultaneous Photothermal Therapy and Chemotherapy of Cancer Cells. *ACS Appl. Mater. Interfaces* **2016**, *8* (50), 34209−34217.
(41) Musumeci, T.; Ventura, C. A.; Giannone, I.; Ruozi, B.; Montenegro, L.; Pignatello, R.; Puglisi, G. PLA/PLGA nanoparticles for sustained release of docetaxel. *Int. J. Pharm.* **2006**, *325* (1−2), 172−179.
(42) Kenmotsu, H.; Tanigawara, Y. Pharmacokinetics, dynamics and toxicity of docetaxel: Why the Japanese dose differs from the Western dose. *Cancer Sci.* **2015**, *106* (5), 497−504.
(43) Wu, J.; Deng, C.; Meng, F.; Zhang, J.; Sun, H.; Zhong, Z. Hyaluronic acid coated PLGA nanoparticulate docetaxel effectively targets and suppresses orthotopic human lung cancer. *J. Controlled Release* **2017**, *259*, 76−82.
(44) Blumenthal, G. M.; Scher, N. S.; Cortazar, P.; Chattopadhyay, S.; Tang, S.; Song, P.; Liu, Q.; Ringgold, K.; Pilaro, A. M.; Tilley, A.; King, K. E.; Graham, L.; Rellahan, B. L.; Weinberg, W. C.; Chi, B.; Thomas, C.; Hughes, P.; Ibrahim, A.; Justice, R.; Pazdur, R. First FDA approval of dual anti-HER2 regimen: pertuzumab in combination with trastuzumab and docetaxel for HER2-positive metastatic breast cancer. *Clin. Cancer Res.* **2013**, *19* (18), 4911−4916.
(45) van der Zee, J. Heating the patient: a promising approach? *Ann. Oncol* **2002**, *13* (8), 1173−1184.
(46) Chatterjee, D. K.; Diagaradjane, P.; Krishnan, S. Nanoparticle-mediated hyperthermia in cancer therapy. *Ther. Delivery* **2011**, *2* (8), 1001−1014.
(47) Wang, Y.; Wei, G.; Zhang, X.; Xu, F.; Xiong, X.; Zhou, S. A Step-by-Step Multiple Stimuli-Responsive Nanoplatform for Enhancing Combined Chemo-Photodynamic Therapy. *Adv. Mater.* **2017**, *29* (12), 1605357.
(48) Liu, X.; Wu, M.; Hu, Q.; Bai, H.; Zhang, S.; Shen, Y.; Tang, G.; Ping, Y. Redox-Activated Light-Up Nanomicelle for Precise Imaging-Guided Cancer Therapy and Real-Time Pharmacokinetic Monitoring. *ACS Nano* **2016**, *10* (12), 11385−11396.
(49) Wei, T.; Chen, C.; Liu, J.; Liu, C.; Posocco, P.; Liu, X.; Cheng, Q.; Huo, S.; Liang, Z.; Fermeglia, M.; Pricl, S.; Liang, X. J.; Rocchi, P.; Peng, L. Anticancer drug nanomicelles formed by self-assembling amphiphilic dendrimer to combat cancer drug resistance. *Proc. Natl. Acad. Sci. U. S. A.* **2015**, *112* (10), 2978−2983.
(50) Baker, J.; Ajani, J.; Scotte, F.; Winther, D.; Martin, M.; Aapro, M. S.; von Minckwitz, G. Docetaxel-related side effects and their management. *Eur. J. Oncol Nurs* **2009**, *13* (1), 49−59.
(51) de Weger, V. A.; Beijnen, J. H.; Schellens, J. H. Cellular and clinical pharmacology of the taxanes docetaxel and paclitaxel–a review. *Anti-Cancer Drugs* **2014**, *25* (5), 488−494.

NOTE ADDED AFTER ASAP PUBLICATION

This paper published ASAP on August 23, 2019 with incorrect versions of Figures 5 and 6 due to a production error. The corrected paper reposted to the Web on September 9, 2019.

DOI: 10.1021/acsbiomaterials.9b01145
ACS Biomater. Sci. Eng. 2019, 5, 4463−4473